Newcastle University

ePrints

**Gibson J, Penfold T.**

**Nonadiabatic Coupling Reduces the Activation Energy in Thermally Activated Delayed Fluorescence.**

***Physical Chemistry Chemistry Physics* 2017**

**DOI: https://doi.org/10.1039/C7CP00719A**

**Copyright:**

This is the authors' accepted manuscript of an article that was published in its final definitive form by Royal Society of Chemistry, 2017.

**DOI link to article:**

https://doi.org/10.1039/C7CP00719A

**Date deposited:**

09/03/2017

**Embargo release date:**

07 March 2018


This work is licensed under a Creative Commons Attribution-NonCommercial 3.0 Unported License

**Newcastle University ePrints - eprint.ncl.ac.uk**

Journal Name

ARTICLE TYPE

Cite this: DOI: 10.1039/xxxxxxxxxx

# Nonadiabatic Coupling Reduces the Activation Energy in Thermally Activated Delayed Fluorescence†

J. Gibson[a] and T.J. Penfold*[a]

Received Date
Accepted Date

DOI: 10.1039/xxxxxxxxxx

www.rsc.org/journalname

The temperature dependent rate of a thermally activated process is given by the Arrhenius equation. The exponential decrease in the rate with activation energy, which this imposes, strongly promotes processes with small activation barriers. This criterion is one of the most challenging during the design of thermally activated delayed fluorescence (TADF) emitters used in organic light emitting diodes. The small activation energy is usually achieved with donor-acceptor charge transfer complexes. However, this sacrifices the radiative rate and is therefore incommensurate with the high luminescence quantum yields required for applications. Herein we demonstrate that the spin-vibronic mechanism, operative for efficient TADF, overcomes this limitation. Nonadiabatic coupling between the lowest two triplet states give rise to a strong enhancement of the rate of reserve intersystem crossing via a second order mechanism and promotes population transfer between the $T_1$ to $T_2$ states. Consequently the rISC mechanism is actually operative between initial and final state exhibiting an energy gap that is smaller than between the $T_1$ and $S_1$ states. This contributes to the small activation energies for molecules exhibiting a large optical gap, identifies limitations of the present computational design procedures and provides a basis from which to construct TADF molecules with simultaneous high radiative and rISC rates.

## 1 Introduction

Molecular fluorescence is usually a two step process. An initial absorption giving rise to an electronically excited state followed by the radiative decay of that state or another one of lower energy into the electronic ground state. This is called prompt fluorescence (PF). However, if the fluorescence and non radiative decay rates from this state is a lot less than the rate of intersystem crossing (ISC), then fluorescence may occur by a more complicated route, the triplet manifold. In this case, the $S_1$ state decays via ISC, ultimately ending up in the $T_1$ state. Subsequently, if the phosphorescence and non radiative decay of the triplet state is slow, as expected, and the energy gap between the singlet and triplet states is small enough (normally $\leq 0.2$ eV), then after vibrational thermalisation, a second ISC, often called reverse ISC (rISC) back to the $S_1$ can occur followed by fluorescence. This is known as delayed fluorescence (DF).

The first observation of delayed fluorescence was by Perrin *et al.*[1] who reported two long-lived emission bands in solid uranyl salts naming them *true phosphorescence* and *fluorescence of long duration*. This was later characterised in more detail by Lewis *et al.*[2] in rigid media and Parker *et al.*[3] using Eosin. The latter study is responsible for the original name, E-type delayed fluorescence, which is now most commonly referred to as Thermally Activated Delayed Fluorescence (TADF).

To achieve efficient TADF, which is desirable for their application as emitters in OLEDs[4,5], one must satisfy the key condition of a small energy gap between the singlet and triplet excited states involved in the rISC, ($\Delta E_{ST}$):

$$k_{rISC} = A \exp\left[\frac{-\Delta E_{ST}}{k_b T}\right]. \quad (1)$$

Molecules with a small singlet-triplet energy splitting are relatively easy to achieve using covalently linked electron donor (D) and acceptor (A) units, and consequently such molecules have become the focus of molecular architectures adopted for TADF. Using this approach, one obtains low lying singlet and triplet excited states with strong charge transfer (CT) character. These are characterised by a very small orbital overlap between the highest occupied molecular orbital (HOMO) and lowest unoccupied molecular orbital (LUMO), assuming these states are predominantly HOMO→LUMO transitions. This minimises the exchange electron energy and therefore the energy gap[6,7].

To date, design of TADF molecules has largely focused upon minimising this energy gap, and therefore the HOMO-LUMO orbital overlap. This is justified when adopting the equilibrium

[a] *School of Chemistry, Newcastle University, Newcastle upon Tyne, NE1 7RU, United Kingdom. tom.penfold@ncl.ac.uk*

† Electronic Supplementary Information (ESI) available: [details of any supplementary information available should be included here]. See DOI: 10.1039/b000000x/

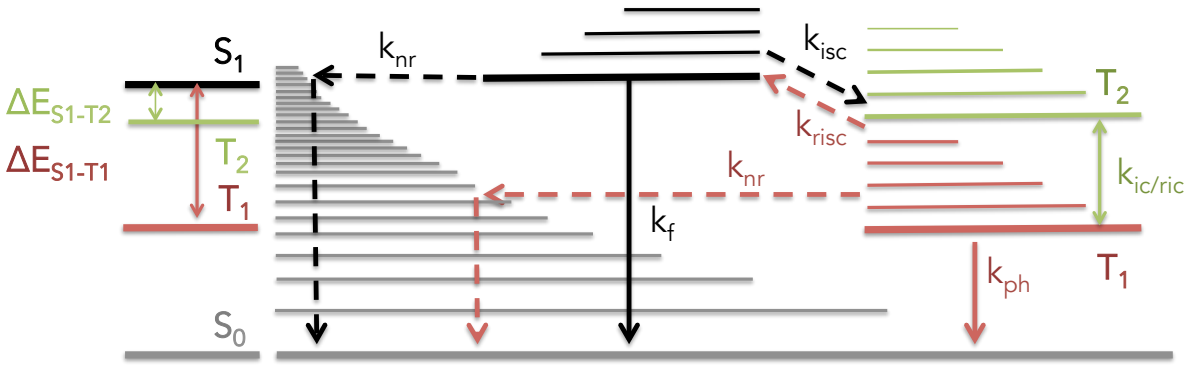


**Fig. 1** Simplified energy diagram representing a general schematic of the low lying singlet and triplet states involved in TADF and other competing processes. $k_f$ and $k_p$ are the fluorescence and phosphorescence rates, respectively. $k_{nr}$ represents non-radiative excited state decay and $k_{ic/ric}$ is the rate of (reserve) internal conversion between the triplet states. $\Delta E_{T_1S_1}$ is the energy gap between the $T_1$ ($^3$LE) and $S_1$ ($^1$CT) state, considered most important in TADF. $\Delta E_{S_1T_2}$ is the energy gap between the $S_1$ ($^1$CT) and $T_2$ ($^3$CT) states.

model for TADF, first proposed by Parker *et al.*[3] and later used by Kirchhoff *et al.*[8]. This regime assumes that $k_F << k_{rISC}$, and in this limit the steady state populations of the emitting singlet and triplet states are determined by Boltzmann statistics, as the molecule spends sufficient time in the excited state for a equilibrium to form before emission eventually occurs. The relative population of the two states can be expressed using an equilibrium constant:

$$K = \frac{[S_1]}{[T_1]} = \frac{k_{rISC}}{k_{ISC}} = \frac{1}{3}\exp\left[\frac{-\Delta E_{S_1T_1}}{k_BT}\right] \quad (2)$$

making it possible to express the rate of the whole TADF process ($k_{TADF}$), i.e. rISC proceeded by fluorescence as the product of the amount of population in the $S_1$ state and the rate limiting step, i.e. $k_F$;

$$k_{TADF} = \frac{1}{3}k_F\exp\left[\frac{-\Delta E_{S_1T_1}}{k_BT}\right] \quad (3)$$

This removes the importance of any effects, other than the energy gap to rISC, provided the coupling between the states is non-zero. However, while this represents a convenient approach for the analysis of photophysical data, the key assumption, i.e $k_{rISC} >> k_F$, must be and often is broken to support new emitters with stronger fluorescence yields[9,10]. Within this regime, TADF must be cast in terms of a kinetic process and therefore opens the question as to what other effects, such as molecular geometry, the dielectric medium, the presence of low energy triplet excited states, localised in the D or A units, contribute to $k_{rISC}$. This makes understanding the rISC process far more involved than simply determining an energy gap between the singlet and triplet CT states[11].

Towards achieving a detailed understanding of the key excited state properties leading to efficient TADF, D-A and D-A-D molecular systems[10,13,14] have been used to demonstrate that the two excited states involved in the rISC step can be independently tuned by changing the local embedding environment. They must therefore be of different character and a $^1$CT and local excitonic triplet ($^3$LE) pair was proposed. Extending this, it was proposed that efficient rISC occurs via a second order spin-vibronic coupling mechanism[15–17], which is analogous to the superexchange mechanism identified in wide variety of artificial light harvesting systems[18–20]. In this case, it is not just the initial and final states, $^3$LE ($T_1$) and $^1$CT ($S_1$), but also an intermediate state, a $^3$CT ($T_2$) state, which is crucial to the rate of rISC. This mechanism was confirmed using a combination of photoinduced absorption and quantum dynamics by exploiting the temperature dependent polarity a host polymer, polyethylene oxide. In this work, the temperature dependent polarity was exploited to bring the charge-transfer states into and out of energetic resonance with the $^3$LE state[12] and shows that TADF reaches a maximum at the resonance point consistent with our proposed spin-vibronic coupling model[15].

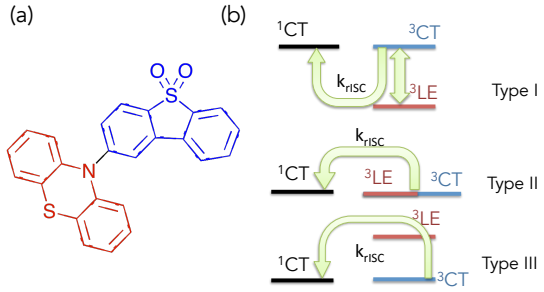


**Fig. 2** (a) Schematic representation of the donor-acceptor (D-A) molecule studied herein. It is composed of a phenothiazine donor and a dibenzothiophene-S,S-dioxide acceptor (PTZ-DBTO2). (b) Schematic energy levels diagrams illustrating the three type of emitter, TADF I (CT>LE), TADF II (CT=LE), and TADF III (CT<LE)[12].

These results also allowed three distinct regimes of present TADF emitter to be categorised, as illustrated in Figure 2. These highlight that, within this regime, there is not just one, but two energy gaps to consider when optimising TADF molecules *. Experimentally to elucidate the gap, $\Delta E_{S_1-T_1}$, there are two ap-

* Strictly speaking there are three energy gaps, but once two are defined, the third is fixed.


This journal is © The Royal Society of Chemistry [year]

proaches adopted. The first is obtained by fitting the integrated DF emission as a function of temperature[10] and therefore gives a thermal activation ($\Delta E_a^{TADF}$) derived from the Arrhenius equation. The second is defined as the difference between the onset of the fluorescence to phosphorescence signals and is therefore the optical gap. Importantly, it has been repeatedly found that the gap extracted from these two approaches are different, sometimes by a much as 0.35 eV[10]. Indeed, larger differences were generally found for the higher performing molecules. Dias *et al.*[10] proposed that this difference could be due to the presence of an intermediate state and therefore the spin-vibronic mechanism discussed in the previous paragraph. Alternatively, Adachi et al.[21] have proposed that this difference is due to conformational changes occurring during the rather long transient lifetime of the triplet excited state. Here, coordinate dependent vibronic coupling, on-diagonal rather than nonadiabatic, alters the adiabatic energy gap between the $T_1$ and $S_1$ states. This corresponds to the strong coupling limit in the pioneering paper of Englman and Jortner[22].

In this paper, we perform a theoretical study on the effect of nonadiabatic couplings for $k_{rISC}$ and in particular on $\Delta E_a^{TADF}$, i.e. the activation energy of TADF. We show the relative importance of the various energy gaps within the spin-vibronic mechanism for TADF and demonstrate that the presence of the intermediate state can reduce the effective activation barrier. This explains the differences in the energy barrier reported from different experimental measurements, and why they tend to emerge most strongly for higher performing molecules. This work highlights the importance of considering nonadiabatic coupling when trying to understand and design efficient TADF emitters, highlights limitations of present design procedures and provides a framework for design TADF molecules with simultaneous high radiative and rISC rates.

The computational details are reported in the supporting material. The model spin-vibronic coupling used throughout, has previously been described in refs.[12,15].

## 2 Results and Discussion

Figure 3 shows the dependency of the rISC on the strength of the nonadiabatic coupling. This illustrates that significant enhancements of $k_{rISC}$ can be achieved by increasing this coupling, with the largest change observed between $\sim 30 \times Q_i$ cm$^{-1}$ and $\sim 130 \times Q_i$ cm$^{-1}$ (i.e. half and double the nonadiabatic coupling calculated in ref.[15]). $Q_i$ is the magnitude of the displacement of wavepacket along normal mode $i$. It is interesting to note that this enhancement is larger when the energy gap between the $T_1$ and $T_2$ states is larger, illustrating the importance of nonadiabatic coupling for enabling rISC for molecules exhibiting larger energy gaps. This is because this spin-allowed coupling is significantly stronger than the other couplings, such as spin-orbit, in the Hamiltonian. Within first order perturbation theory the mixing between the $T_1$ and $T_2$ states can be expressed:

$$T_2 = T_2 + \lambda T_1 \tag{4}$$

where:

$$\lambda = \frac{\langle T_2 | \hat{H}_{vib} | T_1 \rangle}{\Delta E_{T_1 - T_2}} \tag{5}$$

$\hat{H}_{vib}$ is the nonadiabatic coupling operator. This means, assuming $Q_i$=1, that the onset of the rapid increase in $k_{rISC}$ occurs between $\lambda \sim$0.1-0.5. This upper limit illustrates the significant mixing between the $T_1$ and $T_2$.

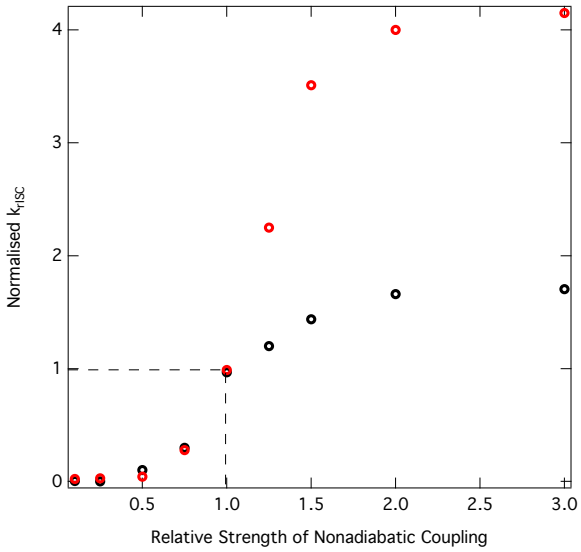


**Fig. 3** The relative rate of reverse intersystem crossing obtained from the quantum dynamics simulations as a function of the strength of nonadiabatic coupling for two models: $\Delta E_{S_1-T_1}$=0.06 (black) and 0.1 eV (red). In both cases $\Delta E_{S_1-T_2}$=0.03 eV. All other parameters of the Hamiltonian are fixed as described in the supporting material.

The effect of increasing the nonadiabatic coupling is a larger mixing between the $T_1$ ($^3$LE) and $T_2$ ($^3$CT) states. Regardless of temperature, mixing between the two states gives rise to some population transfer. The extent of this mixing depends, as shown in Equation 5, on the coupling strength and energy gap. This is consistent with recent results of Ogiwara *et al.*[23] who used electron paramagnetic resonance (EPR) spectroscopy to probe the population of the $^3$LE and $^3$CT states. By fitting the transient experimental signals, they reported that complexes showing the largest rISC exhibited an EPR signal consistent with a mixture of both the $^3$LE and $^3$CT states. The authors used this to propose that efficient rISC not only includes the SOC pathway ($^3$LE$\rightarrow^1$CT), but also a hyperfine coupling induced ISC pathway ($^3$CT$\rightarrow^1$CT). Although this coupling may become operative if the $^1$CT and $^3$CT gap becomes very small (<1 meV), the weak nature of this coupling means that it is too small to account for the experimental rISC rates. In contrast, the spin-vibronic mechanism shows that the larger population of the $^3$CT is associated with a larger $k_{rISC}$ via the strong second-order coupling[12,15].

As shown in Figure 2 the presence of three states driving efficient rISC means that two, rather than one energy gap becomes important. Given the differences between the optical gap and activation energies determined experimentally, as discussed in the introduction, it is important to investigate the effect of each of these to $k_{rISC}$. If one uses the equilibrium model for TADF shown in Equation 3, the effect of a third state can easily be included, by defining two equilibrium constants. A first equilibrium between

the triplet states:

$$K_1 = \frac{[T_2]}{[T_1]} = \frac{k_{rIC}}{k_{IC}} = \exp\left[\frac{-\Delta E_{T_2T_1}}{k_BT}\right], \quad (6)$$

and a second between the $T_2$ and $S_1$ states, active in the spin-vibronic picture:

$$K_2 = \frac{[S_1]}{[T_2]} = \frac{k_{rISC}^{S_1-T_2}}{k_{ISC}^{S_1-T_2}} = \frac{1}{3}\exp\left[\frac{-\Delta E_{S_1T_2}}{k_BT}\right] \quad (7)$$

The whole TADF process ($k_{TADF}$) is now the product of two equiliriums and the rate of fluorescence, $k_F$.

$$\begin{aligned} k_{TADF} &= k_F K_1 K_2 = \frac{1}{3}k_F \exp\left[\frac{-\Delta E_{T_2T_1}}{k_BT}\right]\exp\left[\frac{-\Delta E_{S_1T_2}}{k_BT}\right] \\ &= \frac{1}{3}k_F \exp\left[\frac{-\Delta E_{S_1T_1}}{k_BT}\right] \end{aligned} \quad (8)$$

This is the same as Equation 3 and consequently, the activation energy recorded in both situations should be the same, $\Delta E_{S_1-T_1}$. Behaviour will also determined by Boltzmann statistics, unless other external factors play a role. However external factors, such as nonadiabatic coupling, do play a crucial role, and it is its impact which is now discussed.

Figure 4a shows the normalised $k_{rISC}$ as a function of $\Delta E_{S1-T1}$ and $\Delta E_{T1-T2}$. Half of the plot is excluded as it corresponds to $\Delta E_{T1-T2} > \Delta E_{S1-T1}$, not possible within the one electron limit. Clearly, the rate is largest when both gaps are smallest. This is unsurprising as the near degeneracy promotes strong mixing between the states. As the gaps increase the rate decays exponentially as expected from Equation 1, i.e. as the gap becomes larger, thermal activation is reduced. This is highlighted in Figure 4b showing the exponential decrease $k_{rISC}$ as a function of $\Delta E_{S1-T1}$ with a fixed $\Delta E_{T1-T2}$=0.01 eV.

At larger values of $\Delta E_{S1-T1}$ (Figure 4a), the $k_{rISC}$ is largest for larger $\Delta E_{T1-T2}$, suggesting that efficient rISC occurs when $\Delta E_{S1-T2}$ is smallest. This is confirmed in Figure 4c showing $k_{rISC}$ as a function of $\Delta E_{T1-T2}$ for fixed $\Delta E_{S1-T1}$=0.1 eV. In other words, $\Delta E_{S1-T2}$ dominates over the $\Delta E_{T1-T2}$, which is unexpected as a smaller latter gap promotes stronger nonadiabatic mixing (Equation 5). To explain this, we emphasise the mechanism for efficient rISC. As discussed in ref.[12,15], it is expressed using two terms, one a first order and the other second-order perturbation theory:

$$k_{rIC} = \frac{2\pi}{\hbar}\left|\langle \Psi_{^3CT}|\hat{H}_{vib}|\Psi_{^3LE}\rangle\right|^2 \delta(E_{^3CT} - E_{^3LE}) \quad (9)$$

and

$$k_{rISC} = \frac{2\pi}{\hbar}\left|\frac{\langle \Psi_{^1CT}|\hat{H}_{soc}|\Psi_{^3LE}\rangle\langle \Psi_{^3LE}|\hat{H}_{vib}|\Psi_{^3CT}\rangle}{E_{^3CT} - E_{^3LE}}\right|^2 \delta(E_{^1CT} - E_{^3LE}) \quad (10)$$

Firstly, the large nonadiabatic coupling between $^3$LE and $^3$CT (Equation 9) promotes, on a timescale much faster than the rISC, an equilibrium between the two states. Obviously, the position of this equilibrium depends both on the size of the nonadiabatic coupling and the $\Delta E_{T1-T2}$ energy gap. Subsequently, the second

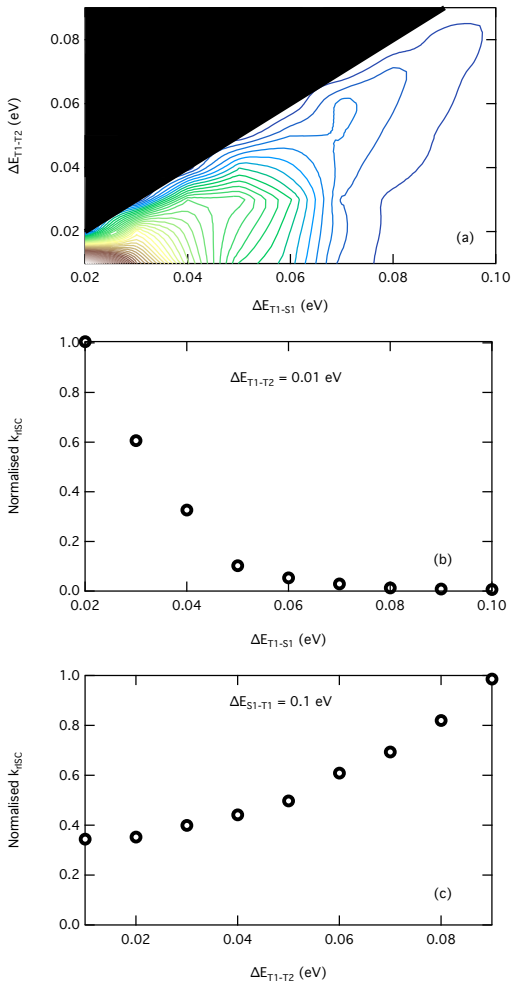


**Fig. 4** (a) Normalised (to the maximum) $k_{rISC}$ as a function of $\Delta E_{S_1-T_1}$ and $\Delta E_{T_1-T_2}$. Half of the plot is excluded as it corresponds to $\Delta E_{T1-T2} > \Delta E_{S1-T1}$. (b) Cut of (a) for $\Delta E_{T_1-T_2}$ = 0.01 eV. (c) Cut of (a) for $\Delta E_{S_1-T_1}$ = 0.1 eV.

order term, Equation 10, couples the $^3$CT and the $^1$CT, using the $^3$LE as an intermediate state. This latter second order term is very efficient because of the good vibrational overlap between the almost degenerate initial and final states, $^3$CT and $^1$CT, respectively.

Adopting a similar approach used for singlet fission[24], these equations can also be cast in a semiclassical (Marcus-like) approach, with a first order terms expressed:

$$k_{rIC} = \frac{2\pi}{\hbar}|\mathscr{V}_{T_1-T_2}|^2 \times \exp\left[-\frac{(\Delta E_{T_1-T_2}+\lambda)^2}{4\lambda k_BT}\right] \quad (11)$$

and second order written:

$$k_{rISC} \sim \frac{2\pi}{\sqrt{2\pi\hbar^2\lambda k_bT}}\frac{|\mathscr{V}_{S_1-T_1-T_2}|^2}{[E_{T2}-E_{T1}]^2} \times \exp\left(-\frac{[\Delta E_{T_2-S_1}+\lambda]^2}{4\lambda k_BT}\right) \quad (12)$$

Here, $\mathscr{V}_{T_1-T_2}$ is the nonadiabatic coupling and $\mathscr{V}_{S_1-T_1-T_2}$ is the second order coupling connecting $T_2$ and $S_1$ via $T_1$. It is noted that these are strictly only valid for the weak coupling limit and we are therefore neglecting the coordinate dependent vibronic cou-


This journal is © The Royal Society of Chemistry [year]

pling which leads to the displacement of excited state minima as discussed above[22]. The implications and contribution of this is discussed in more detail below. In terms of the energy gaps, Equation 11 exhibits a exponential dependence upon the $T_1$-$T_2$ gap, while the second-order rate depends exponentially on the $S_1$-$T_2$ energy gap and quadratically on the $T_1$-$T_2$ energy gap.

Returning to Figure 4c, the reason $k_{rISC}$ increases for larger $\Delta E_{T1-T2}$ is the aforementioned exponential dependence on the $S_1$-$T_2$ energy gap on the second order term. This shows that Equation 12 is clearly dominating the rISC mechanism. Indeed, although a similar exponential dependence is observed in Equation 11 for the mixing between the $T_1$ and $T_2$ states, because the coupling is stronger it appears to be less susceptible to the changes in the energy gap over the range considered here.

To determine the activation energy for rISC from these simulations, Figure 6a shows an Arrhenius plot, $ln(k_{rISC})$ plotted against 1000/K, for two scenarios. The first (black trace) has $\Delta E_{S_1-T_1}$=0.06 eV and $\Delta E_{T_1-T_2}$=0.03 eV. The second (red trace) $\Delta E_{S_1-T_1}$=0.10 eV and $\Delta E_{T_1-T_2}$=0.03 eV. For the latter case, the magnitude of nonadiabatic coupling has been doubled to enable these simulations to exhibit sufficient population transfer to $S_1$ ($^1$CT) at lower temperatures (225 K) within the timescale of our simulations. It is stressed that this has no impact on the conclusions discussed below. Importantly, they both show activation energies that are significantly smaller than the $S_1$-$T_1$ energy gap, 0.04 and 0.03 eV, respectively. In addition, the simulations for $\Delta E_{S_1-T_1}$= 0.06 eV (black trace), which find an activation energy 0f 0.03 eV, are consistent with those reported in ref.[25] on PTZ-DBTO2, for which this model Hamiltonian is based. In this work, the authors reported an energy gap, using the onset of the fluorescence and phosphorescence bands of 0.05 eV and an activation energy of 0.02 eV.

This can be understood using the population of the $^3$CT state as a function of temperature, shown in Figure 6b for the first simulation ($\Delta E_{S_1-T_1}$=0.06 eV and $\Delta E_{T_1-T_2}$=0.03 eV). This shows that the first step, population transfer from $T_1$-$T_2$ is predominantly not thermally activated. This is because while 27% of the wavepacket is in the $T_2$ at 300 K, 20% still remains at 0 K and therefore must simply arises from the presence of state mixing arising from strong nonadiabatic coupling. This is to say that 74% (0.2/0.27) of the wavepacket in the $^3$CT ($T_2$) at 300K populates the upper state purely on the basis on nonadiabatic coupling and independent of temperature. Indeed, the strength of the coupling and the small energy gap between the states means that population transfer between the two states to form, very rapidly (<10 ps)[15], an equilibrium between the two states is possible even at low temperatures. Temperature, depending on the size of the energy gap, will only alter the position of the equilibrium as observed in Figure 5b.

For the fraction of the wavepacket, which is not thermally activated and populates the $T_2$ based only on the nonadiabatic coupling, the energy gap reflected as $E^a_{TADF}$ is purely that of Equation 12, i.e. the energy gap between initial and final states is $S_1$-$T_2$ which is smaller than the $S_1$-$T_1$ (0.03 eV against 0.06 eV). It is emphasised that because both pathways (thermally and non-thermally activated rIC) are clearly possible in this case, the effective activation energy is a combination of both, i.e. an activation of 0.06 eV (combination of Equations 11 and 12) and 0.03 eV (purely Equation 12). Hence the overall activation energy found in Figure 6a is 0.04 eV. For the latter, the larger nonadiabatic coupling and energy gap means that the population of $T_2$ is temperature independent over the range considered. Therefore $E^a_{TADF}$ only reflects the non-thermally activated rIC pathway and therefore the activation energy corresponds to that in Equation 12, and therefore $\Delta E_{S_1-T_2}$=0.03 eV.

This shows for the first time, that nonadiabatic coupling can reduce the activation energy in TADF and can be responsible for the different energy gaps reported for the optical gap and $E_a$. It is emphasised that while these simulations show the important effect the intermediate state has on the rate and $E_a$ in TADF, this does not exclude the sampling of different energy gaps due to molecular conformational changes during the rather long transient lifetime of triplet excitons as proposed by Adachi et al.[21]. Indeed, as discussed above, this work does not incorporate the effect of coordinate dependent vibronic coupling, on-diagonal rather than nonadiabatic. This, as discussed by Adachi et al. modifies the

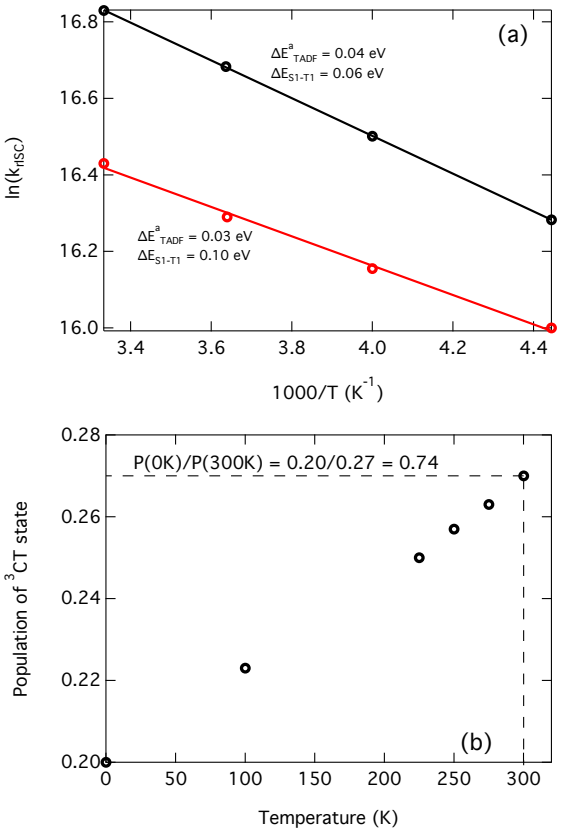


**Fig. 5** (a) Energy barrier for TADF, determined from the temperature variation of $k_{rISC}$ plotted against 1000/T ($K^{-1}$) for two models which have $\Delta E_{S_1-T_1}$=0.06 and 0.1 eV. In the case of the latter, the magnitude of nonadiabatic coupling has been doubled to enable these simulations to exhibit sufficient population transfer to $S_1$ at lower temperatures (225 K). (b) Population of the $T_2$ state as a function of temperature for $\Delta E_{S_1-T_1}$=0.06 eV. For the latter model, the population of $T_2$ is temperature independent over the range considered.

adiabatic energy gap between the $T_1$ and $S_1$ states meaning the wavepacket can access regions of the potential where the energy gap is smaller, promoting rISC at a distorted geometry. This corresponds to the strong coupling limit in the pioneering paper of Englman and Jortner[22]. We expect that to some extent both will be operative. However, as it is desirable to minimise the reorganisation energy in these emitters for high device performance, this nonadiabatic mechanism does offer an alternative design route, previously unknown. Indeed, we show that the rISC mechanism is dynamic, in the sense that it depends on molecular vibrations. Using this to adopt an idea of dynamic molecular optimisation, exploiting nonadiabatic coupling, is general and will have great ramifications in many different fields of molecular photophysics.

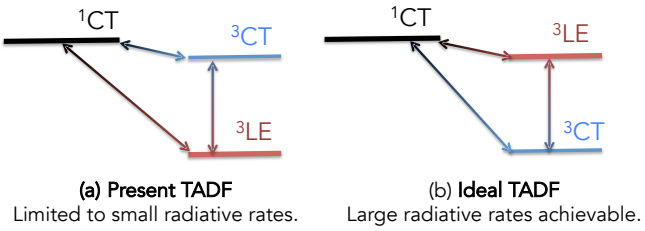


**Fig. 6** (a) Schematic energy level diagram for Type I TADF emitters. (b) Schematic of proposed energy level diagram for higher performing TADF emitters.

## 3 Conclusions

In this paper we have demonstrated the effect of nonadiabatic coupling on $k_{rISC}$ and its importance to the performance of TADF emitters. This coupling provides a second-order pathway, which significantly enhances $k_{rISC}$. The nonadiabatic coupling forms an equilibrium between the two lowest triplet states, $T_1$ ($^3$LE) and $T_2$ ($^3$CT), which leads to significant population transfer, even without thermal activation. This has the effect of lowering the activation barrier for TADF because, according to second-order perturbation theory, it becomes dominated by the $S_1$-$T_2$ energy gap, rather than the $S_1$-$T_1$ energy gap.

Crucially, these results leads us to propose a new approach for designing efficient TADF emitters, shown in Figure 6. Figure 6a shows a schematic energy level diagram for present Type I TADF emitters, such as PTZ-DBTO2. In the previous sections we have shown that the $S_1$-$T_2$ energy gap is most important. However, because these states are of the same character this gap, assuming for simplicity a HOMO→LUMO transitions, can only be small by reducing the overlap between the HOMO and LUMO orbitals, i.e. making them stronger CT transitions. This will come at the cost of the radiative rate, incommensurate with a high luminescence quantum yield. Conversely, if as shown in Figure 6b, the molecule is designed so that the $^1$CT is degenerate with the $^3$LE, then one can relax the condition of a small overlap between the HOMO-LUMO. The excited states of weaker CT character will exhibit a bigger singlet-triplet splitting, but as $^1$CT and $^3$LE are degenerate, efficient TADF will still be achieved. Importantly, in this case because the singlet state is a weaker CT state, it will exhibit a larger radiative rate, leading to the ideal combination of efficient TADF and short radiative lifetimes.

### Computational Details

The Hamiltonian used in the present work is reported in ref.[12,15]. It is composed of 3 electronics states, two charge transfer states ($^1$CT and $^3$CT) and a local exciton state on the donor group, terms $^3$LE. There are 3 nuclear degrees of freedom, which are responsible for the nonadiabatic coupling. The quantum dynamics were performed using a density operator formalism of the multi-configurational time-dependent Hartree (MCTDH) methods[26]. We have adopted a closed quantum system, this is to say that no dissipative operators are included and only the core Hamiltonian. Further details are given in the supporting material.

### Data availability.

Data supporting this publication is openly available under an 'Open Data Commons Open Database License'. Additional metadata are available at: 10.17634/153015-1. Please contact Newcastle Research Data Service at rdm@ncl.ac.uk for access instructions.


### Acknowledgements.

TJP acknowledges the EPSRC, Project EP/N028511/1 for funding.


## References


1 R Delorme and F Perrin. *J. Phys. Rad. Ser.*, 10:177–186, 1929.

2 GN Lewis, D Lipkin, and TT Magel. *J. Am. Chem. Soc.*, 63:3005–3018, 1941.

3 CA Parker and CG Hatchard. *Trans. Faraday Soc.*, 57:1894–1904, 1961.

4 H Uoyama, K Goushi, K Shizu, H Nomura, and C Adachi. *Nature*, 492:234–238, 2012.

5 K Goushi, K Yoshida, K Sato, and C Adachi. *Nature Photonics*, 6:253–258, 2012.

6 A Endo, M Ogasawara, A Takahashi, D Yokoyama, Y Kato, and C Adachi. *Adv. Mater.*, 21:4802–4806, 2009.

7 T J Penfold. *J. Phys. Chem C*, 119:13535?13544 (2014).

8 KR Kirchhoff, R E Gamache, M W Blaskie, A A Del Paggio, R K Lengel, and D R McMillin. *Inorg. Chem.*, 22:2380–2384, 1983.

9 Q Zhang, J Li, K Shizu, S Huang, S Hirata, H Miyazaki, and C Adachi. *J. Am. Chem. Soc*, 134:14706–14709, 2012.

10 F B Dias, K N Bourdakos, V Jankus, K C Moss, K T Kamtekar, V Bhalla, J Santos, M R Bryce, and A P Monkman. *Adv. Mater.*, 25(27):3707–3714, 2013.

11 F B Dias, TJ Penfold, and A P Monkman. *Methods Appl Fluoresc*, in press, 2017.

12 MK Etherington, J Gibson, HF Higginbotham, Penfold TJ, and AP Monkman. Nature Comm. 7:13680 2016.

13 JS Ward, R S Nobuyasu, A S Batsanov, P Data, A P Monkman,





This journal is © The Royal Society of Chemistry [year]

F B Dias, and M R Bryce. *Chem. Commun.*, 52:2612-2615 2016.

14 P L Santos, J S Ward, P Data, A S Batsanov, M R Bryce, F B Dias, and A P Monkman. *J. Mater. Chem. C*, 4, 3815-3824 2016.

15 J Gibson, AP Monkman, and TJ Penfold. *ChemPhysChem*, 17:2956-2961 2016.

16 CM Marian *J. Phys. Chem. C*, 120:3715–3721 2016.

17 XK Chen, SF Zhang, JX Fan and A-M Ren, *J. Phys. Chem. C*, 119:9728–9733 2015.

18 S R Yost, J Lee, M WB Wilson, T Wu, D P McMahon, R R Parkhurst, N J Thompson, D N Congreve, A Rao, K Johnson, et al. *Nature Chem.*, 6:492–497, 2014.

19 H Tamura, M Huix-Rotllant, I Burghardt, Y Olivier, and D Beljonne. *Phys. Rev. Lett.*, 115:107401, 2015.

20 M Natali, S Campagna, and F Scandola. *Chem. Soc. Rev.*, 43:4005–4018, 2014.

21 S Hirata, Y Sakai, K Masui, H Tanaka, S Y Lee, H Nomura, N Nakamura, M Yasumatsu, H Nakanotani, Q Zhang, K Shizu, H Miyazaki, and C Adachi. *Nature Mater.*, 14, 330-336 (2015) .

22 R. Englman and J. Jortner *Mol. Phys.*., 18, 145–164 (1970) .

23 T Ogiwara, Y Wakikawa, and T Ikoma. *J. Phys. Chem A*, 119:3415–3418, 2015.

24 T C Berkelbach, M S Hybertsen, and D R Reichman. *J. Chem. Phys.*, 138:114103, 2013.

25 RS Nobuyasu, Z Ren, G C Griffiths, A S Batsanov, P Data, S Yan, A P Monkman, M R Bryce, and F B Dias. *Advanced Optical Materials*, DOI:10.1002/adom.201500689 2016.

26 H-D Meyer and G A Worth. *Theoretical Chemistry Accounts*, 109:251–267, 2003.